

# Chapter 4

## D<sub>s</sub><sup>+</sup> and D<sup>+</sup> reconstruction strategy in proton-proton collisions

Due to their mean proper decay lengths ( $c\tau$ ) of 151.2  $\mu\text{m}$  and 309.8  $\mu\text{m}$  respectively [1], D<sub>s</sub><sup>+</sup> and D<sup>+</sup> mesons and their charge conjugates cannot be directly detected, as they typically decay before reaching the ALICE detector. Consequently, their production is inferred through the reconstruction of their decay products. This analysis exploits their hadronic decays into  $D_s^+(D^+) \rightarrow \phi\pi^+ \rightarrow K^+K^-\pi^+$  and their charge conjugates, with a branching ratio of  $(2.21 \pm 0.06) \times 10^{-2}$   $((2.69^{+0.07}_{-0.08}) \times 10^{-3})$  [1]. An additional hadronic decay channel of the D<sup>+</sup> meson with a larger BR of  $(9.38 \pm 0.16) \times 10^{-2}$  [1] could be exploited [2]. However, the reconstruction of the two D-mesons species in the same decay channel allows for the cancellation of many of the systematic uncertainties affecting the measurement, leading to a more precise D<sub>s</sub><sup>+</sup>/D<sup>+</sup> production yield ratio measurement. The choice of reconstructing D mesons through their decays into a hadronic final state allows for the full reconstruction of the decay topology, therefore providing a more precise measurement. Semileptonic decay measurements are in fact affected by larger uncertainties due to the presence of neutrinos in the final state, which are not detected. In addition, the decay into the resonant  $\phi(1020)$  state opens up the possibility of exploiting the invariant mass of the  $\phi$  meson for the selection of the D-meson candidates. A sketch of the decay topology of D<sub>s</sub><sup>+</sup> and D<sup>+</sup> mesons into  $\phi\pi^+ \rightarrow K^+K^-\pi^+$  is shown in Fig. 4.1.

D<sub>s</sub><sup>+</sup> and D<sup>+</sup> mesons (and their charge conjugates) are reconstructed in three different steps: i. firstly, charged tracks are reconstructed at midrapidity ( $|\eta| < 0.8$ ) exploiting the ITS and TPC detectors; ii. D<sub>s</sub><sup>+</sup> and D<sup>+</sup> candidates are constructed by combining triplets of tracks with the appropriate charge signs, i.e., (+, -, +) for D<sub>s</sub><sup>+</sup> and D<sup>+</sup> mesons, and (-, +, -) for their antiparticles; iii. finally, the D<sub>s</sub><sup>+</sup> and D<sup>+</sup> candidates are selected by applying a set of topological, kinematical, and Particle-IDentification (PID) selections. Given the large number of tracks produced in a pp collision, the vast majority of the constructed D<sub>s</sub><sup>+</sup> and D<sup>+</sup> candidates are obtained from the combination of uncorrelated tracks, which do not originate from the same decay vertex. This results in a large *combinatorial background*, which has to be suppressed in order to extract the signal of the D mesons.

The spatial resolution capabilities of the ALICE detector described in Chap-

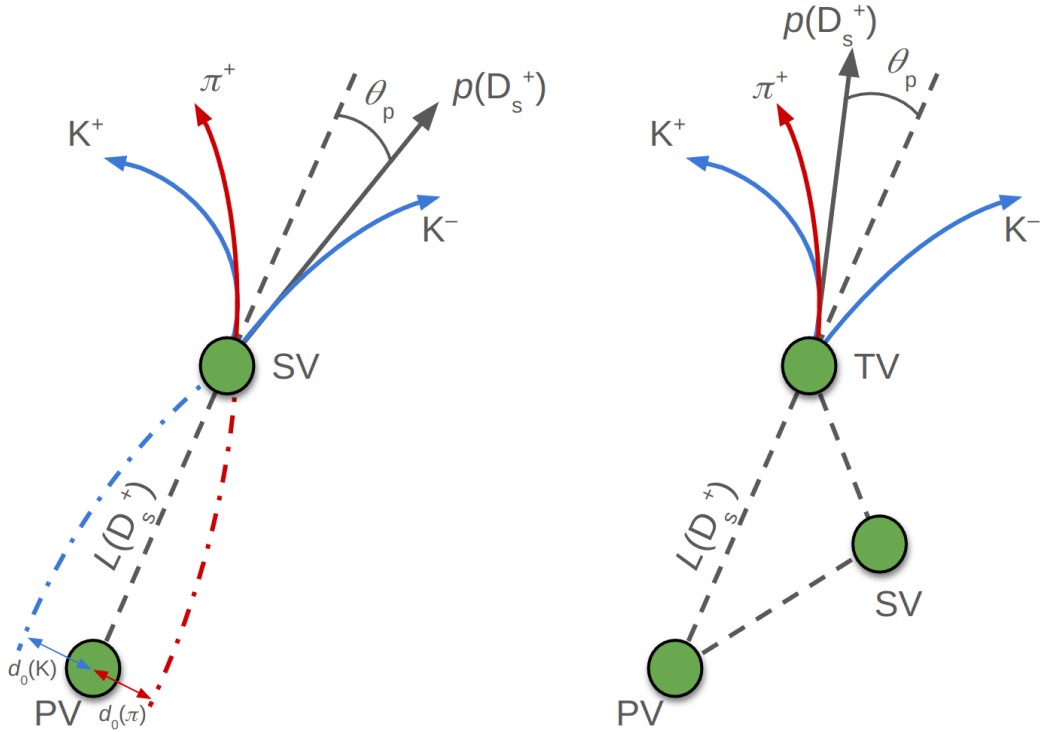


Figure 4.1: Sketch of the decay topology of  $D_s^+$  and  $D^+$  mesons into  $\phi\pi^+ \rightarrow K^+K^-\pi^+$  for prompt (left) and non-prompt (right)  $D_s^+$  meson.

ter ?? enable the separation of the secondary decay vertices of D mesons from the primary interaction vertex, which consents the development of an analysis based on the reconstruction and selection of secondary-vertex topologies characterised by relatively large separations from the primary interaction vertex. Furthermore, PID information can be exploited to improve the selection of D mesons and their decay products and reduce the background.

Two distinct categories of D mesons emerge based on their production mechanism: *prompt* and *non-prompt* (also referred to as *feed-down*). Decay vertices of feed-down D mesons are on average more displaced from the primary interaction point with respect to promptly-produced ones, due to the larger mean proper decay length of beauty hadrons ( $c\tau \sim 500 \mu\text{m}$  [1]) as compared to charm hadrons. Therefore, by exploiting selection criteria based on displaced decay-vertex topologies, it is possible not only to separate D-meson signals from the combinatorial background, but also to discriminate between feed-down and prompt D mesons.

## 4.1 Data sample and event selection

The analysis reported in this Thesis is performed on a dataset of pp collisions at a centre-of-mass energy of  $\sqrt{s} = 13.6 \text{ TeV}$ , collected by the ALICE detector during the 2022 data-taking period. The data sample is collected using a Minimum-Bias trigger (the **Se18** trigger), which selects events that satisfy the requirement of having a signal coincidence in the FT0-A and FT0-C detectors. Furthermore, since it is observed

that the readout of the TPC (which is performed at the end of each TF) causes a drop in the track reconstruction efficiency, it was decided to exclude the collisions read out during this time interval (*TF border* selection). An additional requirement is imposed on the primary vertex position along the beam axis,  $|z_{\text{vtx}}| < 10 \text{ cm}$ , to ensure that the point where protons have collided is located within the region of the detector where the tracking efficiency is optimal. Of the total 59.2 billion collected events, only 54.7 billion have been analysed, corresponding to an integrated luminosity of  $\mathcal{L}_{\text{int}} \sim 1 \text{ pb}$ . Around 3% of the events are rejected due to the minimum bias trigger, about 1% due to the TF border selection, and 4% of the events are rejected due to the requirement on the  $z_{\text{vtx}}$  position. A summary of the event selection is shown in Fig. 4.2.

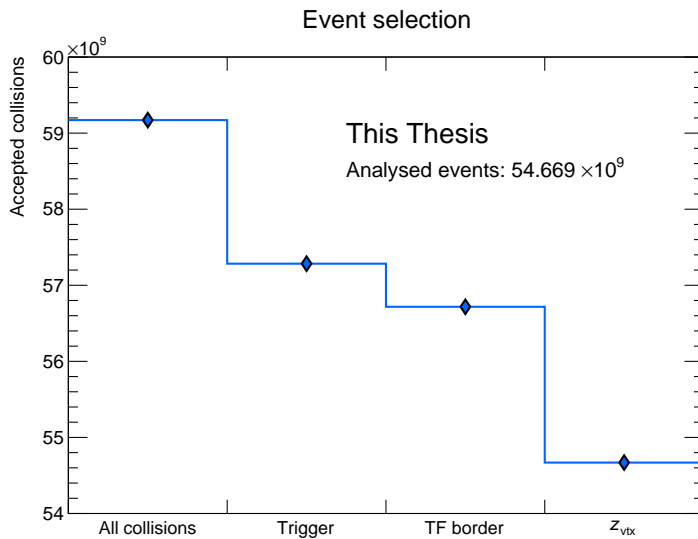


Figure 4.2: Summary of the event selection criteria applied to the data sample.

## 4.2 $D_s^+$ and $D^+$ reconstruction workflow

The reconstruction of  $D_s^+$  and  $D^+$  mesons is a complex process performed in many subsequent steps. As stated in Chapter ??, the reconstructed data are stored in AOD format. This format contains essential information about the reconstructed tracks, which are parameterised at the innermost update point, i.e., the closest point to the primary vertex with a detected track signal. Since the track parametrisation is not the same for each track, as missing hits in the ITS can lead to different radii of the innermost update points, the tracks are propagated to the point of closest approach to the primary vertex, and their parameters are updated accordingly. This procedure is performed in the `track-propagator` workflow, and only tracks passing a set of predefined quality requirements are selected.

Because of continuous readout, there exists the possibility that a single track is found to be compatible with multiple collisions (these tracks are named *ambiguous tracks*). In the AOD files, the ambiguous tracks are only associated with the first

space-time-compatible collision. In order to increase the reconstruction efficiency, the **track-to-collision associator** workflow associates each track with all compatible collisions. This process significantly increases the reconstruction efficiency, especially for 2- or 3-body decaying particles.

For each considered collision, combinations of two or three tracks are built in the **track-index-skim-creator** workflow, which produces a table of track indices for combinations passing a set of loose selection criteria, which depend on the considered hadron species. Candidates for each particle species and their decay vertices are created in the **candidate-creator** workflow, and those passing the more stringent analysis selection criteria are flagged in the **candidate-selector** workflow. The **tree-creator (analysis-task)** workflow produces the final output of the analysis, which consists of a ROOT tree (several ROOT histograms) containing the properties of selected candidates.

### 4.3 $D_s^+$ and $D^+$ decay-vertex reconstruction and selection

The decay vertex of the candidate is reconstructed through a minimisation of a  $\chi^2$ -like quantity, denoted as  $D$ :

$$D = \sqrt{\sum_{i=1}^3 \left[ \left( \frac{x_i - x_0}{\sigma_{x_i}} \right)^2 + \left( \frac{y_i - y_0}{\sigma_{y_i}} \right)^2 + \left( \frac{z_i - z_0}{\sigma_{z_i}} \right)^2 \right]} ,$$

where  $(x_i, y_i, z_i)$  and  $(\sigma_{x_i}, \sigma_{y_i}, \sigma_{z_i})$  represent the position and the uncertainty of the  $i$ -th track at the point of closest approach, respectively, while  $(x_0, y_0, z_0)$  denotes the position of the reconstructed vertex. The invariant mass and momentum of the  $D_s^+$  and  $D^+$  candidates are computed from the energy and momentum of the measured tracks evaluated at the point of closest approach to the decay vertex. The momentum of the candidate is defined as the sum of the momenta of the three tracks. For the invariant mass computation, the kaon mass is always assigned to the track with opposite charge sign with respect to the D-meson candidate (*opposite-sign track*). For the two *like-sign tracks*, the two pion-kaon mass hypothesis combinations (i.e.  $(K^+ K^- \pi^+)$  and  $(\pi^+ K^- K^+)$  for positively charged candidates) are considered.

The vast majority of the created  $D_s^+$ - and  $D^+$ -meson candidates belong to the large combinatorial background. To increase the signal-over-background ratio and the statistical significance of the measurement, tight selections are required to suppress such candidates. The analyses presented in this Thesis exploit several selection criteria, which can be divided into:

- i Track-quality selections
- ii Selections based on the decay topology and kinematics
- iii Particle identification of the decay products

In the following, the variables used to select D mesons and some of the applied selections are described in more detail.

### 4.3.1 Track-quality selections

Only tracks that successfully pass strict quality and kinematic requirements are considered eligible for inclusion in the construction of  $D_s^+$ - and  $D^+$ -meson candidates. In particular, only ITS-TPC tracks with at least 70 (out of a maximum of 159) track-associated space points in the TPC, and a crossed rows (i.e., the total number of hit TPC pad rows) over findable clusters (i.e., pad rows that could potentially be hit, given the track’s trajectory) ratio of at least 0.8 are selected. To improve the vertex reconstruction procedure, at least one hit in the 3 innermost layers of the ITS, which compose the ITS inner barrel, was required.

Secondary vertices of  $D_s^+$ - and  $D^+$ -meson candidates are constructed using tracks having  $|\eta| < 0.8$  and  $p_T > 0.3$  GeV/c. A track-quality requirement of  $\chi^2$  per TPC cluster smaller than 4 has been applied. A cut on the daughter-track transverse impact parameter projection in the transverse plane  $d_0^{xy}$  was applied, requiring  $d_0^{xy} > 25 \mu\text{m}$  for tracks with  $p_T < 2$  GeV/c. These selections limit the rapidity acceptance of D mesons, which steeply decreases for  $|y| > 0.5$  at low  $p_T$  and for  $|y| > 0.8$  for  $p_T \gtrsim 5$  GeV/c, as shown in Fig. 4.3. The applied track-quality selection criteria are summarised in Table 4.1.

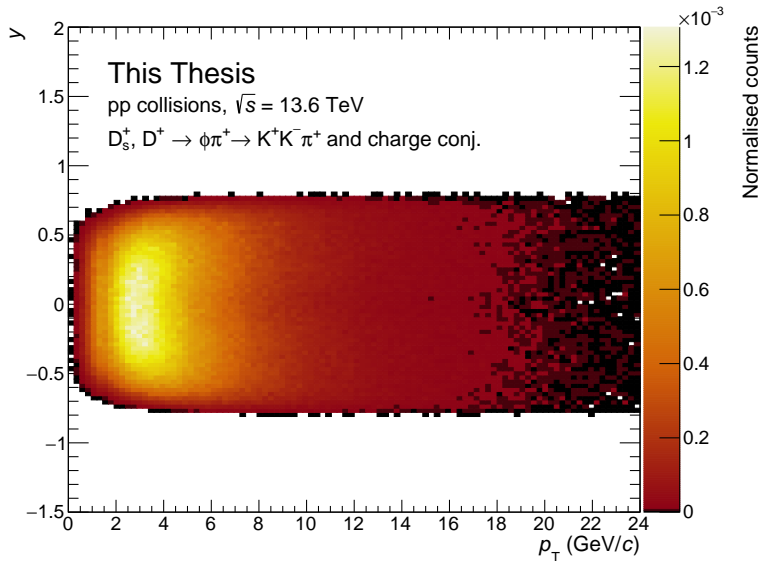


Figure 4.3: Rapidity and transverse momentum distribution of reconstructed  $D_s^+$  and  $D^+$  mesons in pp collisions at  $\sqrt{s} = 13.6$  TeV.

### 4.3.2 Topological selections

$D_s^+$  and  $D^+$  mesons exhibit a displaced decay vertex topology, which can be used to separate the signal from the uninteresting combinatorial background. Moreover, promptly produced D mesons exhibit different topological features compared to feed-down D mesons, enabling further discrimination between the two production mechanisms. This differentiation potentially offers insights into beauty-quark production through the measurement of open-charm states.

Single-track selection	Value
Number of TPC crossed-rows >	70
$ \eta  <$	0.8
$p_T >$	0.1 $\text{GeV}/c$
$\chi_{\text{TPC}}^2/\text{TPC clusters} <$	4
$\chi_{\text{ITS}}^2/\text{ITS clusters} <$	36
ITS matching	At least 1 cluster in L0, L1, L2

Table 4.1: Applied single-track selection criteria

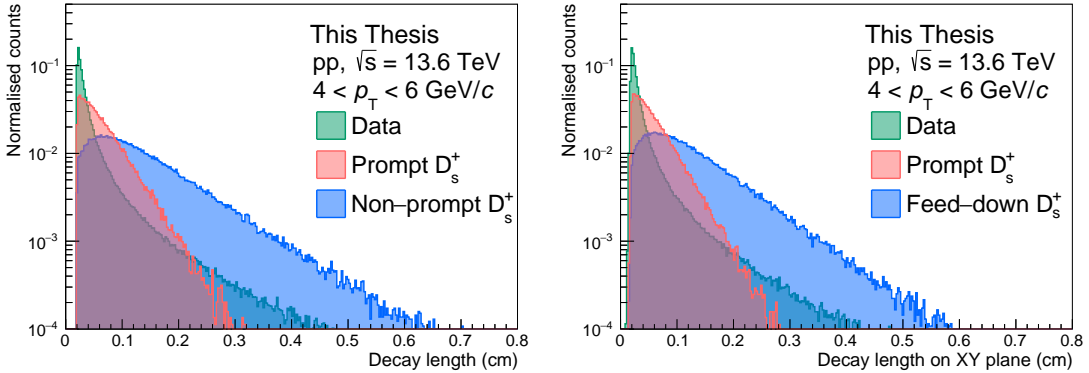


Figure 4.4: Distributions of decay length (left panel) and its projection on the transverse plane (right panel) for  $D_s^+$  mesons in pp collisions at  $\sqrt{s} = 13.6 \text{ TeV}$  in the  $4 < p_T < 6 \text{ GeV}/c$  interval. The distributions are shown for prompt  $D_s^+$  mesons (blue), non-prompt  $D_s^+$  mesons (orange), and combinatorial background (green). For prompt and non-prompt  $D_s^+$  mesons, the distributions are taken from Monte Carlo simulations, whereas for combinatorial background they are taken from the data sidebands.

The topological selections are tuned as a function of  $p_T$  in order to increase the signal-over-background and the statistical significance of the measurement. The different selections are presented herein. The corresponding distributions of variables are shown for the signal, which is divided into prompt and feed-down contributions and obtained from Monte Carlo simulations, as well as for the combinatorial background, which is obtained from real data in an invariant-mass region away from the signal region, denoted as *sidebands* and chosen as  $1.7 < M < 1.75 \text{ GeV}/c^2$  or  $2.1 < M < 2.15 \text{ GeV}/c^2$ .

## Decay Length

The decay length  $L$  is defined as the distance between the primary and secondary vertices. It provides an approximation of the actual decay length of  $D_s^+$  and  $D^+$  mesons, as the particle's curvature resulting from the motion in the presence of a magnetic field is not considered. However, given the small mean proper decay length of  $\sim 150$  ( $310$ )  $\mu\text{m}$  of  $D_s^+$  ( $D^+$ ) mesons, this effect can be neglected.

This is one of the most important variables used to distinguish between signal and combinatorial background, since the displaced topology of the signal shifts the decay length distribution towards larger values. Furthermore, since beauty-hadron decay vertices are not reconstructed, the measured decay length of non-prompt D-mesons also accounts for the decay length of their parent hadrons. As a consequence, the resulting decay length distribution for feed-down D-mesons is particularly shifted towards larger values, allowing for an easier separation of this production mechanism from the background. The distribution of the decay length also depends on the D-meson  $p_T$ , because of the Lorentz boost which contributes to an increase in the distance flown by the hadron measured in the laboratory reference frame. Moreover, since the mean proper decay length of  $D^+$  meson is about twice as large as that of the  $D_s^+$  meson, the decay length distribution of the former is shifted towards larger values. This allows for a possible discrimination of the two D-meson species based on the exclusive exploitation of topological variables.

In addition to the decay length, its projection on the transverse plane can also be used to select  $D_s^+$  or  $D^+$  signal. This variable is particularly useful as it exploits the better resolution of the ALICE experiment in the transverse plane with respect to the longitudinal one. Previous measurements of D mesons also leveraged the normalised decay length, defined as the ratio between the decay length and its uncertainty, to further improve the signal extraction. Although this variable demonstrated a good separation power, it was not used in this analysis, due to possible biases introduced by the uncertainty description in the Monte Carlo simulations.

The distributions of decay length and its projection on the transverse plane are shown in Fig. 4.4 for signal and combinatorial background candidates reconstructed in the  $4 < p_T < 6$  GeV/ $c$  interval.

### Cosine of pointing angle

The pointing angle  $\theta_p$  is defined as the angle between the flight direction of the D meson, obtained from the line connecting the primary and secondary vertices, and the direction of the reconstructed D-meson momentum. This variable can also be defined using only the transverse components of these quantities ( $\theta_p^{xy}$ ), to exploit the better resolution in the  $x$  and  $y$  coordinates than in the  $z$  coordinate. In an ideal scenario where particles' momentum is perfectly reconstructed, the cosine of the pointing angle for promptly-produced D mesons would be equal to 1, while that of feed-down D mesons would be distributed around 1, but with a tail towards lower values as the flight direction of the D meson is not equal to that of the parent beauty hadron. On the contrary, the pointing angle for combinatorial background could assume any value with the same probability. The pointing angle is therefore particularly useful to separate the signal from the combinatorial background. The distributions of the cosine of the pointing angle and its projection on the transverse plane are shown in Fig. 4.5 for signal and combinatorial background candidates reconstructed in the  $4 < p_T < 6$  GeV/ $c$  interval. Due to the finite resolution of the tracking detectors, the pointing angle is not perfectly reconstructed, leading to a distribution of the cosine of the pointing angle for prompt  $D_s^+$  that is peaked at 1, but with a tail towards lower values.

Similarly to the decay length, also  $\theta_p$  evolves with the D-meson transverse mo-

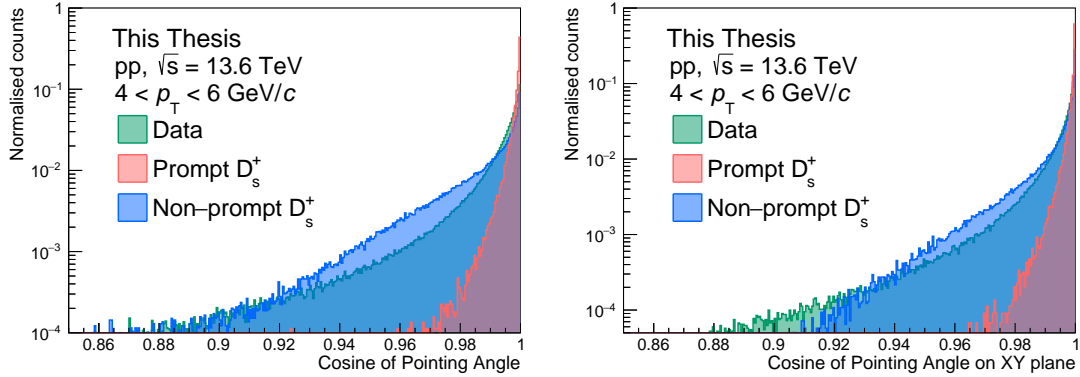


Figure 4.5: Distributions of the cosine of the pointing angle (left panel) and its projection on the transverse plane (right panel) for  $D_s^+$  mesons in pp collisions at  $\sqrt{s} = 13.6$  TeV in the  $4 < p_T < 6$  GeV/ $c$  interval. The distributions are shown for prompt  $D_s^+$  mesons (blue), non-prompt  $D_s^+$  mesons (orange), and combinatorial background (green). For prompt and non-prompt  $D_s^+$  mesons, the distributions are taken from Monte Carlo simulations, whereas for combinatorial background they are taken from the data sidebands.

mentum. Because of the Lorentz boost, the direction of the daughter particles of the D meson is more collimated with the D-meson flight direction at higher  $p_T$ . This results in a distribution of the cosine of the pointing angle that is more peaked at 1 for higher  $p_T$  values.

### Impact parameter in the transverse plane

The projection of the impact parameter on the transverse plane  $d_0^{xy}$  is defined as the distance of closest approach between the reconstructed flight line of the D-meson and the primary vertex, projected in the  $xy$  plane. It is expected to be very close to zero for promptly-produced D mesons, with any deviation due to the detector resolution. Thanks to the better momentum and vertexing resolution, its distribution becomes narrower at high  $p_T$ . It is a powerful variable not only to separate the signal from the combinatorial background, but also to discriminate between prompt and feed-down D mesons, as the latter have a much broader impact parameter distribution, as shown in the left panel of Fig 4.6. In addition, also the projection of the daughter tracks' impact parameter to the primary vertex projected on the transverse plane is used to select the signal. Since the combinatorial background does not have a secondary vertex, many of the tracks used to construct such candidates are produced directly in the primary vertex. This results in a narrow distribution around 0 of the prongs' impact parameters for such candidates. On the contrary, the displaced decay vertex of the signal candidates leads to a broader distribution of the impact parameter for prompt D-meson candidates, and to an even broader one for the non-prompt contribution to the signal, as shown in the right panel of Fig. 4.6.

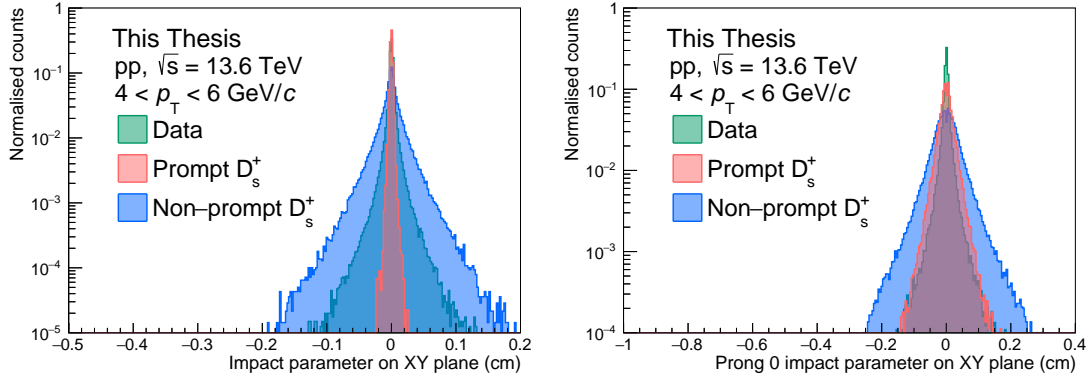


Figure 4.6: Distributions of the projection of the impact parameter on the transverse plane for  $D_s^+$  mesons (left panel) and for one of the opposite-sign daughter tracks (right panel) in pp collisions at  $\sqrt{s} = 13.6$  TeV in the  $4 < p_T < 6$   $\text{GeV}/c$  interval. The distributions are shown for prompt  $D_s^+$  mesons (blue), non-prompt  $D_s^+$  mesons (orange), and combinatorial background (green). For prompt and non-prompt  $D_s^+$  mesons, the distributions are taken from Monte Carlo simulations, whereas for combinatorial background they are taken from the data sidebands.

### 4.3.3 Kinematic selections

In addition to the selections based on the decay topology, kinematic selections are also applied to increase the signal-over-background ratio and the statistical significance of the measurement.

#### Difference between reconstructed and PDG mass of the $\phi$ meson

This selection exploits the production of an intermediate resonant  $\phi(1020)$ -meson state in the considered decay channel of the D mesons, whose invariant mass of  $M_\phi = (1019.461 \pm 0.016)$   $\text{MeV}/c^2$  [1] is known with good precision. The  $K^+K^-$  pair produced in the  $\phi$ -meson decay is expected to have an invariant mass very close to the PDG value, as the  $\phi$  resonance is narrow ( $\Gamma_\phi = 4.249 \pm 0.013$   $\text{MeV}/c^2$  [1]). Therefore, the difference between the reconstructed and the PDG mass of the  $\phi$  meson  $|\Delta M(KK)|$  is expected to be close to zero for signal candidates, while the distribution for combinatorial background is expected to be uniformly distributed.

Moreover, two possible  $K^+K^-$  pairs can be built for each triplet of tracks, depending on the mass hypothesis assigned to the like-sign tracks (e.g., for a  $D_s^+$  decay, both the  $K^+K^-\pi^+$  and  $\pi^+K^-K^+$  mass hypotheses can be considered). Both hypotheses are considered in the reconstruction, and the selection on  $|\Delta M(KK)|$  results extremely helpful not only in rejecting the combinatorial background, but also the reflections, i.e., D mesons with wrongly-assigned mass hypothesis on the decay tracks.

The distribution of this variable is shown in the left panel of Fig. 4.7 for signal and combinatorial background candidates reconstructed in the  $4 < p_T < 6$   $\text{GeV}/c$  interval.

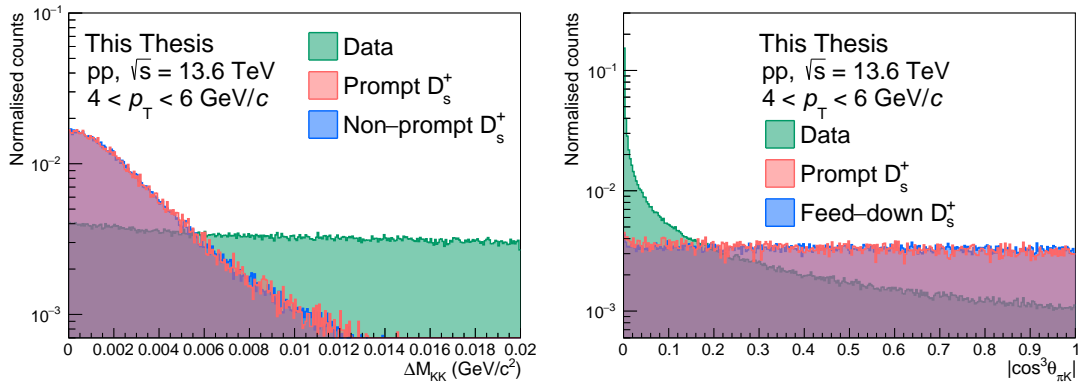


Figure 4.7: Distributions of the difference between the reconstructed and PDG mass of the  $\phi$  meson (left panel) and the cosine cubed of the  $K-\pi$  angle in the KK rest frame (right panel) for  $D_s^+$  mesons in pp collisions at  $\sqrt{s} = 13.6$  TeV in the  $4 < p_T < 6$   $\text{GeV}/c$  interval. The distributions are shown for prompt  $D_s^+$  mesons (blue), non-prompt  $D_s^+$  mesons (orange), and combinatorial background (green). For prompt and non-prompt  $D_s^+$  mesons, the distributions are taken from Monte Carlo simulations, whereas for combinatorial background they are taken from the data sidebands.

### Cosine cubed of the $K-\pi$ angle in the KK rest frame

The decay of a (pseudoscalar) D-meson to a (vector)  $\phi$ -meson and a (pseudoscalar)  $\pi^+$  final state results in an alignment of the spin of the  $\phi$  meson transverse to the direction of motion of the  $\phi$  relative to the D-meson, due to elicity conservation [3]. As a consequence, the distribution of  $\cos(\theta'(K))$ , where  $\theta'(K)$  is the angle between one of the kaons and the pion in the  $K^+K^-$  rest frame, follows a  $\cos^2(\theta'(K))$  shape, which in turn implies a flat distribution for the  $\cos^3(\theta'(K))$  variable, in case of signal. In contrast, the combinatorial background has a flat distribution for  $\cos(\theta'(K))$ , and its  $\cos^3(\theta'(K))$  distribution peaks at zero. This variable is particularly useful to separate the signal from the combinatorial background, as shown in the right panel of Fig. 4.7.

#### 4.3.4 Particle identification selections

One of the distinctive features of the ALICE detector are the excellent PID capabilities in a wide range of momentum, achieved by combining the information from different detectors.

The ITS was used for its PID information during the LHC Run 1 and Run 2 data-taking periods, when the analogue readout of the SDD and SSD layers allowed for the measurement of the specific energy loss  $dE/dx$  of charged particles from the charge deposited in the detector. The upgraded ITS 2 is not capable of providing such information, as the readout is now fully digital. Nonetheless, new PID techniques based on ML algorithms exploiting information such as the cluster shape and size are being developed and tested for the ITS 2. Preliminary results show that the ITS 2 PID is capable of achieving a good separation between protons and other particles, as shown in the left panel of Fig. 4.8.

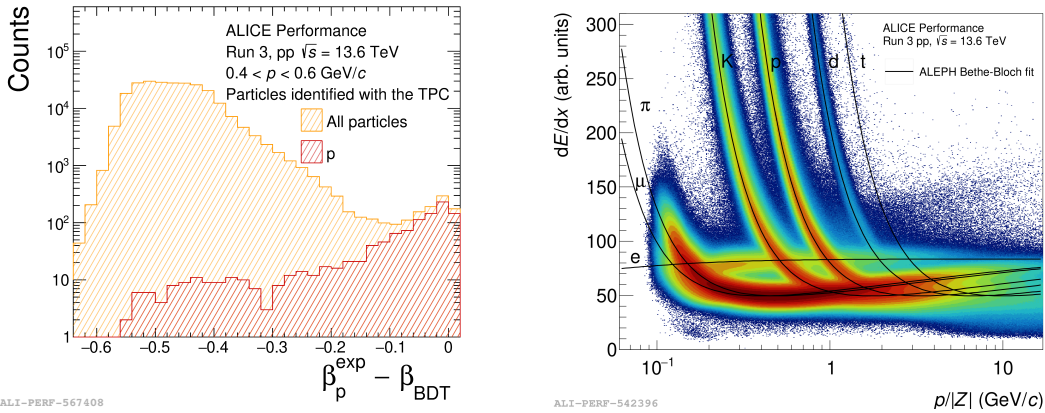


Figure 4.8: Left: ITS 2 particle identification performance in pp collisions at  $\sqrt{s} = 13.6$  TeV using a Boosted Decision Tree (BDT) regressor. From the cluster size, the regressor predicts the velocity  $\beta$  ( $\beta_{\text{BDT}}$ ) of particles. The regressor performance is evaluated for  $0.4 < p < 0.6$  GeV/ $c$ , through the difference between  $\beta_{\text{BDT}}$  and  $\beta_p^{\text{exp}} = \frac{p}{\sqrt{p^2+m_p^2}}$ . Right: Specific energy loss distribution  $dE/dx$  in the TPC for pp collisions at  $\sqrt{s} = 13.6$  TeV. The curves obtained with a fit using the ALEPH parametrisation of the Bethe-Bloch formula for electrons, muons, pions, kaons, protons, deuterium and tritium are also shown. Figures taken from the ALICE figure repository [4].

The TPC is the main PID detector in the ALICE experiment, as it provides a simultaneous measure of the specific energy loss via the charge produced in the drift volume and deposited in its 159 pad rows, the charge, and the momentum of each particle traversing the detector gas. A truncated mean of the  $dE/dx$  samples is calculated discarding the 40% highest-charge clusters, which ensures the removal of the Landau tail of the  $dE/dx$  distribution caused by  $\delta$ -rays, which are produced from the ionisation of the gas by the electrons produced in the primary ionisation. The particle identification is based on the comparison of the measured  $dE/dx$  with the expectation for a specific particle species with a certain momentum  $p$ . The expected  $dE/dx$  is described by the Bethe-Bloch formula, and is typically parametrised with a function originally proposed by the ALEPH collaboration [5]:

$$f(\beta\gamma) = \frac{P_1}{\beta^{P_4}} \left[ P_2 - \beta^{P_4} - \log \left( P_3 + \frac{1}{(\beta\gamma)^{P_5}} \right) \right] .$$

In this parametrisation,  $\beta$  and  $\gamma$  are the particle velocity and Lorentz factor, respectively, and  $P_{1-5}$  are the parameters of the fit function. The  $dE/dx$  distribution in the TPC is shown in the right panel of Fig. 4.8 for pp collisions at  $\sqrt{s} = 13.6$  TeV. The curves obtained with a fit using the ALEPH parametrisation of the Bethe-Bloch formula for electrons, muons, pions, kaons, protons, deuterium and tritium are also shown. While in the non-relativistic low momentum region ( $p \leq 1$  GeV/ $c$ )  $p$ ,  $K$  and  $\pi$  can be separated on a track-by-track basis, at higher momenta, in the relativistic rise region, particles can still be identified on a statistical basis via multi-Gaussian fits. This is possible because the truncated-mean method produces a  $dE/dx$  peak

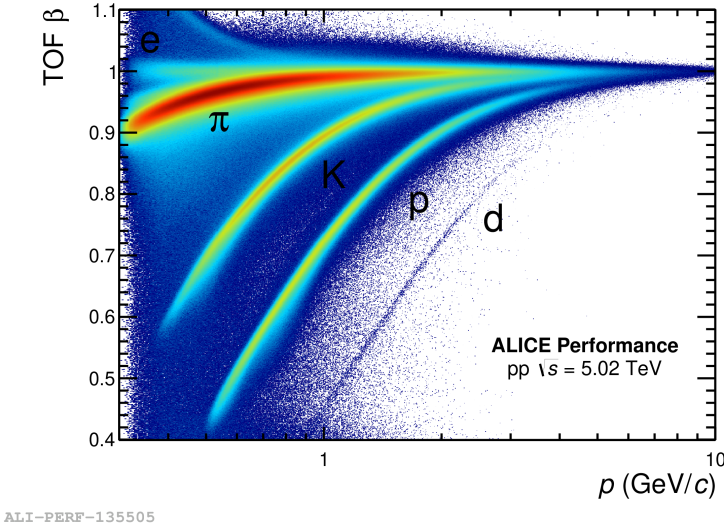


Figure 4.9:  $\beta$  parameter measured with the TOF detector as a function of the momentum  $p$  measured by the TPC detector in Pb–Pb collisions at  $\sqrt{s_{\text{NN}}} = 5.02$  TeV. Figure taken from the ALICE figure repository [4].

with a gaussian shape down to three orders of magnitude for long tracks (at least 130 clusters) [6].

The TOF detector is dedicated to PID in the intermediate momentum range, up to 2.5 GeV/ $c$  for pions and kaons, and up to 4 GeV/ $c$  for protons. In this higher- $p_T$  region, the TPC is not able to provide a sufficient separation between the different particle species. The TOF detector is based on the measurement of the time of flight of charged particles between the interaction point and the detector. The start time is provided by the FT0 forward-rapidity detectors, and a total time resolution of the 80 ps is achieved, allowing for a separation of the different particle species based on the time of flight. The TOF PID performance is shown in Fig. 4.9 for Pb–Pb collisions at  $\sqrt{s_{\text{NN}}} = 5.02$  TeV. The large background is due to tracks that are incorrectly matched to TOF hits in high-multiplicity Pb–Pb collisions.

Other detectors, such as the High Momentum Particle Identification Detector (HMPID) or the Transition Radiation Detector (TRD), complement the PID capabilities of the ALICE experiment. The HMPID is dedicated to the identification of particles with momenta above 2 GeV/ $c$ , and is based on the detection of Cherenkov radiation emitted by charged particles traversing a radiator. The TRD is used for the identification of electrons and positrons, and is based on the detection of transition radiation emitted by charged particles traversing a radiator with a change in the dielectric constant. The TRD is particularly useful for the identification of electrons and positrons in the high-multiplicity environment of heavy-ion collisions, where the TPC and TOF detectors are not able to provide a sufficient separation between electrons and pions.

The PID information on the decay tracks can be exploited to improve the background rejection and thereby the signal extraction. For this analysis, only the information from the TPC and TOF detector is used, as the ITS PID capabilities

are still under development, and the final state particles of the D mesons are pions and kaons, which can be well identified with the TPC and TOF detectors. A track is considered compatible with a mass hypothesis (i.e. a hadron species) depending on the difference between the measured signal  $S_{\text{meas}}^{\text{TPC,TOF}}$  and the expected signal  $S_{\text{exp}(\pi,\text{K},p)}^{\text{TPC,TOF}}$  for the given hypothesis. The measured signal is the truncated mean of the  $dE/dx$  distribution for the TPC detector, and the time of flight for the TOF detector. The expected signal is extracted from the ALEPH parametrisation of the Bethe-Bloch formula described above for the TPC, and from a parametrisation of the distribution of  $\beta$  as a function of  $p$  for the TOF. The difference between the measured and expected signals is then usually normalised by the uncertainty on the measured signal  $\sigma_{\text{TPC,TOF}}$ :

$$n\sigma_{\pi,\text{K},p}^{\text{TPC,TOF}} = \frac{|S_{\text{meas}}^{\text{TPC,TOF}} - S_{\text{exp}(\pi,\text{K},p)}^{\text{TPC,TOF}}|}{\sigma_{\text{TPC,TOF}}}.$$

Tracks are considered if at least one PID signal is available from one of the two detectors. A loose preselection is applied to the candidates based on PID information, requiring the three tracks to have a  $n\sigma^{\text{TPC}} < 5$ , or  $n\sigma^{\text{TOF}} < 5$  for the considered mass hypothesis. This selection effectively reduces the amount of reflections in the data sample, as the wrongly-assigned mass hypothesis are often rejected.

Due to a TPC–TOF matching efficiency which is significantly lower than unity, the PID information from the two detectors is typically combined to obtain a single PID variable  $n\sigma_{\pi,\text{K},p}^{\text{comb}}$ , which is used in the final selection. The PID information is combined as

$$n\sigma_{\pi,\text{K},p}^{\text{comb}} = \begin{cases} n\sigma_{\pi,\text{K},p}^{\text{TOF}} & \text{only TOF information is available} \\ n\sigma_{\pi,\text{K},p}^{\text{TPC}} & \text{only TPC information is available} \\ \frac{1}{\sqrt{2}} \sqrt{(n\sigma_{\pi,\text{K},p}^{\text{TPC}})^2 + (n\sigma_{\pi,\text{K},p}^{\text{TOF}})^2} & \text{otherwise} \end{cases}$$

This reduces the number of features used for the Machine Learning analysis described in the following Chapters, and ensures a proper handling of sparse data.

# Bibliography

- [1] **Particle Data Group** Collaboration, R. L. Workman and Others, “Review of Particle Physics”, *PTEP* **2022** (2022) 083C01.
- [2] **ALICE** Collaboration, S. Acharya *et al.*, “Measurement of D-meson production at mid-rapidity in pp collisions at  $\sqrt{s} = 7$  TeV”, *Eur. Phys. J. C* **77** (2017) 550, [arXiv:1702.00766 \[hep-ex\]](https://arxiv.org/abs/1702.00766).
- [3] **ATLAS** Collaboration, G. Aad *et al.*, “Measurement of  $D^{*\pm}$ ,  $D^\pm$  and  $D_s^\pm$  meson production cross sections in  $pp$  collisions at  $\sqrt{s} = 7$  TeV with the ATLAS detector”, *Nucl. Phys. B* **907** (2016) 717–763, [arXiv:1512.02913 \[hep-ex\]](https://arxiv.org/abs/1512.02913).
- [4] **ALICE** Collaboration, “ALICE Figure.”  
<https://alice-figure.web.cern.ch/>.
- [5] W. Blum, L. Rolandi, and W. Riegler, *Particle detection with drift chambers. Particle Acceleration and Detection*. 2008.
- [6] **ALICE** Collaboration, B. B. Abelev *et al.*, “Performance of the ALICE Experiment at the CERN LHC”, *Int. J. Mod. Phys. A* **29** (2014) 1430044, [arXiv:1402.4476 \[nucl-ex\]](https://arxiv.org/abs/1402.4476).